

Designing Kitaev spin liquids in metal-organic frameworks

Masahiko G. Yamada,¹ Hiroyuki Fujita,¹ and Masaki Oshikawa¹

¹*Institute for Solid State Physics, University of Tokyo, Kashiwa 277-8581, Japan.*

(Dated: March 8, 2022)

Kitaev's honeycomb lattice spin model is a remarkable exactly solvable model, which has a particular type of spin liquid (Kitaev spin liquid) as the ground state. Although its possible realization in iridates and α - RuCl_3 has been vigorously discussed recently, these materials have substantial non-Kitaev direct exchange interactions and do not have a spin liquid ground state. We propose metal-organic frameworks (MOFs) with Ru^{3+} (or Os^{3+}) forming the honeycomb lattice as promising candidates for a more ideal realization of Kitaev-type spin models where the direct exchange interaction is strongly suppressed. The great flexibility of MOFs allows generalization to other three-dimensional lattices, for potential realization of a variety of spin liquids such as a Weyl spin liquid.

PhySH: Frustrated magnetism, Spin liquid, Quantum spin liquid, Organic compounds

Introduction. — Quantum spin liquids, purported exotic states of quantum magnets where long-range magnetic orders are destroyed by quantum fluctuations, have been a central subject in quantum magnetism [1]. As an important theoretical breakthrough, Kitaev constructed a spin-1/2 model on the honeycomb lattice [2] with Ising interactions between spin components depending on bond orientations. Its exact solution demonstrates many intriguing properties such as fractionalized anyonic excitations. This model was later generalized to other lattices, including three-dimensional ones, still retaining the exact solvability [3]. In this paper, we call this type of model including various generalizations as Kitaev model, and its ground states as Kitaev spin liquids.

Jackeli and Khaliullin [4] discovered that the “Kitaev interaction”, namely bond-dependent Ising couplings, can be realized in a (111) honeycomb layer of iridates, i.e. the $A_2\text{IrO}_3$ ($A = \text{Na}, \text{Li}$) structure, by the superexchange interaction through the oxygen ions due to the strong spin-orbit coupling of Ir^{4+} in the Mott insulator limit (see also Ref. [5] for the itinerant limit).

However, unfortunately, it turned out that iridates and related inorganic compounds, such as α - RuCl_3 [6], exhibit a conventional magnetic order at low enough temperatures and do not have a true spin liquid ground state. This is due to the non-Kitaev interactions, such as antiferromagnetic Heisenberg interaction, mainly coming from the direct exchange interaction between the metal ions [7]. While their finite-temperature properties still reflect the proximity to the Kitaev model [8] and thus are of great interest, the current situation calls for a more ideal realization of the Kitaev model in real materials, so that they exhibit spin liquid ground states.

In this Letter, we propose such a possible realization of the Kitaev model in metal-organic frameworks (MOFs), crystalline materials consisting of metal ions and bridging organic ligands. Although MOF is a central subject in modern complex chemistry, MOFs have not attracted much attention in the context of magnetism. This is

perhaps because they do not show any magnetic ordering at room temperature as direct exchange interactions between magnetic metal ions are suppressed and the remaining indirect superexchange interactions via nonmagnetic organic ligands are weak. We take the advantage of this suppression of direct exchange interactions to realize the Jackeli-Khaliullin mechanism, i.e. superexchange realization of the Kitaev interaction. Furthermore, based on tight-binding models and the fragment molecular orbital (fMO) method [9] in combination with the density functional theory (DFT) calculations, we demonstrate that the Jackeli-Khaliullin mechanism gives rise to the dominant Kitaev interactions with oxalate-based (or tetraaminopyrazine-based) ligands. This opens up the possibility of *designing* the appropriate MOFs to realize Kitaev spin liquids.

Structures of the Proposed Metal-Organic Frameworks.

— In order to realize a Kitaev spin liquid in MOFs using the Jackeli-Khaliullin mechanism [4], we first propose an MOF structure with Ru^{3+} (or Re^{2+} , Os^{3+} , Rh^{4+} , Ir^{4+}) ions in the octahedral coordination. Because of the composite effects of the octahedral ligand field and the strong spin-orbit coupling, these $4d^5$ or $5d^5$ ions show a low-spin ground state with an effective angular momentum $J_{\text{eff}} = 1/2$. Hinted by the (111) honeycomb layers of iridates, we propose a geometric structure shown in Fig. 1(a), where the RuO_6 octahedra form a two-dimensional (2D) honeycomb lattice and the organic ligand (in this case oxalate, $(\text{C}_2\text{O}_4)^{2-}$, or ox^{2-}) connects the two edges of the octahedra. Indeed, many honeycomb MOFs with this structure have already been found by chemists [10–21]. More interestingly, this honeycomb structure of metal-oxalate frameworks is also found in nature in the form of minerals, stepanovite and zhemchuzhnikovite [22]. Thus, we can expect that this honeycomb geometry is chemically stable. Moreover, experiments [23] for the molecule $[\{\text{Ru}(\text{acac})_2\}_2(\mu\text{-ox})]^-$ ($\text{acac}^- = \text{acetylacetonate}$) observed an anisotropic spin interaction via oxalate due to the spin-orbit coupling of Ru^{3+}

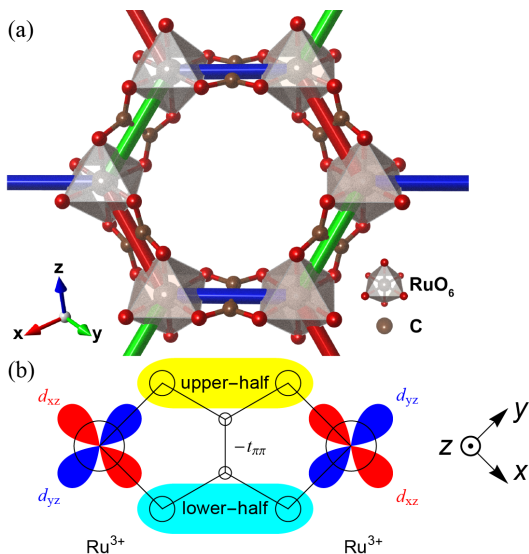


FIG. 1. (Color online) (a) Geometric structure of honeycomb Ru-oxalate frameworks. White octahedra are RuO₆ octahedra and carbon atoms are shown in brown. The color of the bond between the Ru atoms means which plane the bridging oxalate belongs to (red: *yz*-plane, green: *zx*-plane, blue: *xy*-plane). (b) Two superexchange pathways between two neighboring Ru³⁺ through an oxalate ion belonging to the *xy*-plane (one of the blue bonds in (a)). $t_{\pi\pi}$ is a hopping parameter between the two distinct pathways.

with electron spin resonance. Similar anisotropy has also been observed in many other Ru and Os complexes [24]. It is, therefore, natural to consider Ru and oxalate to realize the Kitaev interaction, as the first candidate.

The ligand can be replaced with other organic molecules to achieve a wide variety of MOFs. Some possibilities, including a newly proposed one, are listed in Fig. 2(a) for MOFs with Ru³⁺ (or Os³⁺) in the octahedral coordination. In Fig. 2(a), **1** is oxalic acid ($E = O$) and becomes oxalate in the proposed MOF (see Fig. 2(b)). In the case of $E = S$ (resp. NH), we call it tetrathiooxalate (resp. tetraaminoxalate). Similarly, **2** becomes dhbq²⁻ ($E = O$, $X = H$ and dhbq = 2,5-dihydroxy-1,4-benzoquinone) or X_2An^{2-} ($E = O$, $X = Cl, Br, \text{etc.}$ and An = anilate), and **3** is tetraaminopyrazine C₄N₆H₆ and becomes (C₄N₆H₄)²⁻, which we have newly proposed. There already exists a metal-oxalate framework including Ru³⁺, such as LaRu(ox)₃·10H₂O in Ref. [20], and the molecule [Ru(ox)₃]³⁻ is known to be a good spin-1/2 qubit [25], so it is very natural to use this Ru(ox)₃ unit as a building block for highly entangled quantum states. In any M_2L_3 ($M = Ru, Os$, and $L = ox, dhbq, \text{etc.}$) structures, the metal ion M should be in the 3+ state and the organic ligand L should be in the 2- state. Additional structures may be necessary to maintain the rigid honeycomb structure for M_2L_3 layers, but it will not affect the effective spin model as long as Ru or Os is in the 3+ state and the interlayer interaction is

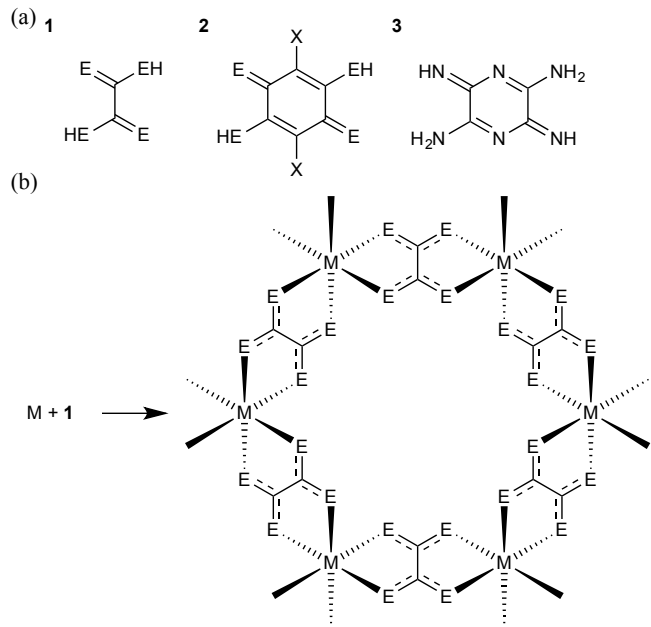


FIG. 2. Chemical formulae for the proposed metal-organic frameworks. (a) Possible organic molecules to realize a honeycomb structure with octahedral coordination. **1**: Oxalate-based molecules ($E = O, S, NH$). **2**: Quinoid-based molecules ($E = O, S, NH; X = H, Cl, Br, I, \text{etc.}$). **3**: Tetraaminopyrazine-based molecule. (b) Honeycomb structure of metal-oxalate frameworks ($M = Ru, Os$).

negligible. In fact, in the Fe³⁺-based MOF with layered structure discovered in Ref. [21], the interlayer distance of metal ions is as large as 8.7449 Å, and the interlayer interaction is found to be negligible or ferromagnetic.

Superexchange Interaction. — The main obstacle to realize Kitaev spin liquids in inorganic materials was the direct exchange interaction between the metal ions, which yields significant non-Kitaev interactions [7]. In MOFs, the electron density of the bridging organic ligand screens the wavefunction tails of the metal ions, which would substantially reduce the direct overlap between orbitals of the neighboring metals. Thanks to this, the direct exchange interaction is strongly suppressed in most MOFs [21]. This is the most important advantage of using organic ligands for the realization of Kitaev spin liquids compared to other inorganic candidates, such as iridates and α -RuCl₃. However, non-Kitaev interactions can also arise from the superexchange interaction. In order to evaluate the magnitude of those terms, we derive the effective spin Hamiltonian in the following steps. First we obtain the effective tight-binding model for the superexchange between two Ru ions, and then we map this model into the effective spin model. As a concrete example, we take one specific bond belonging to the *xy*-plane shown in Fig. 1(b) in the following discussions.

As we will see below, Jackeli-Khaliullin mechanism works perfectly to give rise to the pure Kitaev interac-

tion, if there are two separate superexchange pathways connecting d_{xz} and d_{yz} only. The advantage of using oxalate as the ligand is the existence of the localized modes along upper- and lower- edges of the molecule, which are analogous to the localized edge modes along the zigzag edges of graphene [26]. They can function as the desired two superexchange pathways. In fact, the separation of the two paths is not perfect and we have to consider the effect of their mixing quantitatively. Nevertheless, as we will demonstrate, the mixing is small and the two superexchange pathways are approximately protected. This leads to a dominant Kitaev interaction.

In the chemical terminology, we may consider two “fragment molecular orbitals” (fMO) [9] corresponding to these localized edge modes. For simplicity, here we focus on HOMOs (highest occupied molecular orbitals) and LUMOs (lowest unoccupied molecular orbitals) coming from π -orbitals (π -HOMO and π^* -LUMO for short, respectively), which are the most important as superexchange pathways between Ru^{3+} ions. With the annihilation operators u and l , respectively, for π -HOMOs along upper- and lower-edges in Fig. 1(b), the model Hamiltonian may be written as

$$H_{d\pi} = -t_{d\pi}(u^\dagger d_{yz}^L + l^\dagger d_{xz}^L + u^\dagger d_{xz}^R + l^\dagger d_{yz}^R + h.c.) + V_\pi(u^\dagger u + l^\dagger l) - t_{\pi\pi}(u^\dagger l + l^\dagger u), \quad (1)$$

where $t_{d\pi}$ is the hopping matrix element between the Ru t_{2g} -orbitals and the π -HOMOs, V_π is the energy level of π -HOMOs, $t_{\pi\pi}$ is the tunneling matrix element between the two fMOs, d_i^L (resp. d_i^R) is the annihilation operator of an electron on the Ru d_i -orbital on the left (resp. right) side in Fig. 1(b). Similar terms exist for the π^* -LUMO with the energy level V_{π^*} or the hopping and tunneling matrix elements $t_{d\pi^*}$ and $t_{\pi^*\pi^*}$, respectively. If the separation of the two paths were perfect, then $t_{\pi\pi} = 0$, but in reality it is non-vanishing. Thus the energy levels of HOMOs are split into $V_\pi \pm t_{\pi\pi}$. Nevertheless, reflecting the approximate protection of the two pathways, $t_{\pi\pi}$ is relatively small. This can be confirmed by the DFT calculations, as we will discuss later.

Integrating over the π -HOMO states u and l , we obtain the effective hopping terms between the two Ru^{3+} ions as

$$H_{dd} = -t_1(d_{yz}^L d_{yz}^R + d_{xz}^L d_{xz}^R) - t_2(d_{yz}^L d_{xz}^R + d_{xz}^L d_{yz}^R) - t_3 d_{xy}^L d_{xy}^R + h.c., \quad (2)$$

where $t_1 = t_{d\pi}^2 t_{\pi\pi} / (V_\pi^2 - t_{\pi\pi}^2)$, $t_2 = t_{d\pi}^2 V_\pi / (V_\pi^2 - t_{\pi\pi}^2)$, and $t_3 = 0$. As expected, t_1/t_2 is small when $t_{\pi\pi}$ is small. We should also include the superexchange contributions through π^* -LUMO and σ -orbitals in deriving the effective hopping terms.

Once we obtain the effective hopping (2), by projecting onto $J_{\text{eff}} = 1/2$ states of Ru^{3+} , we can derive the effective

spin model [27]

$$H = \sum_{\langle ij \rangle \in \alpha\beta(\gamma)} [J \mathbf{S}_i \cdot \mathbf{S}_j + K S_i^\gamma S_j^\gamma + \Gamma (S_i^\alpha S_j^\beta + S_i^\beta S_j^\alpha)], \quad (3)$$

where J is the Heisenberg coupling, K is the Kitaev coupling, and Γ is the symmetric off-diagonal exchange. The explicit form of these parameters is included in Supplemental Material. $\alpha, \beta, \gamma \in \{x, y, z\}$ and $\langle ij \rangle \in \alpha\beta(\gamma)$ mean that the bond plane of the nearest-neighbor bond $\langle ij \rangle$ is the $\alpha\beta$ -plane perpendicular to the γ -axis. This model is an extended version of the Kitaev-Heisenberg model [28], known as the JKT model [27, 29]. In the limit $J/|K| \rightarrow 0, \Gamma/|K| \rightarrow 0$, the model is nothing but the honeycomb Kitaev model [2], which has a gapless spin liquid ground state. Here we ignore Dzyaloshinskii-Moriya interactions, assuming the parity symmetry around the bond center.

In this way, we can estimate the parameters J , K , and Γ starting from the fMO-based model (1) of the ligand. As we have emphasized, if the superexchange paths along the upper- and lower- halves were completely separate, $t_{\pi\pi} = t_{\pi^*\pi^*} = 0$ which would give $t_1 = t_3 = 0$. With the effective hopping (2) with only t_2 non-vanishing, Jackeli-Khaliullin mechanism works perfectly and we would obtain the ideal Kitaev model with $J = \Gamma = 0$. This condition could easily be met by using two formates as bridging ions, each of which acts as a separate superexchange pathway, although the honeycomb structure may be unstable in metal-formate frameworks.

Estimation of Spin Interactions. — In order to estimate the parameters in the effective spin model (3) in real MOFs proposed in Fig. 2, we have performed DFT calculations for the oxalate ligand using OPENMX [30] software package. It should be noted that a calculation on a ligand molecule only gives the energy differences such as $V_{\pi^*} - V_\pi$. The individual energy levels such as V_{π^*} and V_π measured from the Fermi level, i.e. the Ru $J_{\text{eff}} = 1/2$ orbital, cannot be directly obtained.

In this work, as a crude but quick estimate to see the potential of our proposal, we will proceed as follows. In the case of oxalate, for example, $V_{\pi^*} - V_\pi = 6.47$ eV from DFT. Experiments [23] suggest that the metal to ligand charge transfer (MLCT) energy $E_{\text{LUMO}} = V_{\pi^*} - t_{\pi^*\pi^*} \sim 2.6$ eV, which corresponds to the optical absorption at the wavelength of 485 nm. This, together with $t_{\pi\pi} = 0.153$ eV and $t_{\pi^*\pi^*} = 1.631$ eV from the DFT calculations, implies $V_{\pi^*} \sim 4.2$ eV and $V_\pi \sim -2.3$ eV. Using these parameters, and $t_{d\pi^*}/t_{d\pi} \sim 0.6159$ for oxalate, we find the ratio between the effective hoppings in Eq. (2) as

$$\frac{t_1}{t_2} = \frac{\frac{t_{d\pi}^2 t_{\pi\pi}}{V_\pi^2 - t_{\pi\pi}^2} - \frac{t_{d\pi^*}^2 t_{\pi^*\pi^*}}{V_{\pi^*}^2 - t_{\pi^*\pi^*}^2}}{\frac{t_{d\pi}^2 V_\pi}{V_\pi^2 - t_{\pi\pi}^2} - \frac{t_{d\pi^*}^2 V_{\pi^*}}{V_{\pi^*}^2 - t_{\pi^*\pi^*}^2}} \sim 0.023. \quad (4)$$

Taking the superexchange via σ -orbitals into account in a similar manner, we find $t_3/t_2 \sim -0.196$. From these

values, we estimate $J/|K| \sim 0.004$ and $|\Gamma|/|K| \sim 0.15$, namely the Kitaev interaction is strongly dominant. The details of the derivation is given in Supplemental Material.

In general, we find that the resulting low-energy effective model is dominated by the Kitaev interaction ($J/|K| \sim |\Gamma|/|K| \lesssim 1/10$), if the conditions $|t_{\pi\pi}|/|V_{\pi}| \lesssim 1/10$ and $|V_{\pi}|/|V_{\pi^*}| \lesssim |t_{d\pi}\sqrt{t_{\pi\pi}}|/|t_{d\pi^*}\sqrt{t_{\pi^*\pi^*}}|$ are both met. We note that the smallness of $|V_{\pi}|/|V_{\pi^*}|$ implies that the superexchange is hole-mediated [31].

Although there is no particular reason to have degeneracy in aromatic ligands, such as $\text{d}h\text{bq}^{2-}$ and X_2An^{2-} (**2** in Fig. 2(a)), it is possible to have similar degeneracy of π -HOMOs in the tetraaminopyrazine-based ligand $(\text{C}_4\text{N}_6\text{H}_4)^{2-}$ (**3** in Fig. 2(a)). In contrast to oxalate, the degenerate two π -HOMOs are just below the Fermi energy even in the vacuum, so tetraaminopyrazine-based structures should also be good candidates for Kitaev-dominant MOFs. In addition, this $(\text{C}_4\text{N}_6\text{H}_4)^{2-}$ would stabilize the planar structure more easily than oxalate due to the π -conjugated nature.

While the present estimate is crude and we have ignored many possible corrections, these results suggest that our proposal of realizing Kitaev spin liquids in MOFs is quite promising. We emphasize that, MOFs have the flexibility in the choice of ligand molecules, so that many possibilities can be tried for the realization of Kitaev spin liquids.

Designing a Variety of Kitaev Spin Liquids. — Here we emphasize another advantage of MOFs: we can construct various complex geometric structures, not limited to the honeycomb lattice, by self-organization. In particular, three-dimensional (3D) generalizations of the Kitaev model are of great interest [32]. A realization in iridates has been reported but again with a magnetic ordering at low temperatures [33]. One of the 3D structures known as the hyperhoneycomb lattice or (10,3)-*b* is, on the other hand, naturally realizable in MOFs, such as $[(\text{C}_2\text{H}_5)_3\text{NH}]_2\text{Cu}_2(\text{C}_2\text{O}_4)_3$ shown in Fig. S1 in Supplemental Material, and can in principle be constructed just by putting building blocks altogether and stirring [34]. The cation-templating is known to be important to construct a 3D structure [34], so we would possibly need to replace Cu^{2+} with Re^{2+} rather than with Ru^{3+} . The analysis in the previous section can also be applied to MOFs with 3D tricoordinated lattices, to derive the same JKT model as the effective low-energy spin model on the corresponding lattice.

By applying a magnetic field to break the time-reversal symmetry, the system with a 3D hyperhoneycomb lattice is expected to show a gapless Weyl spin liquid ground state [35]. More interestingly, there are other 3D tricoordinated lattices with exotic Majorana states, which have not been found in iridates but are possible in 3D MOFs. Among these, the hyperoctagon lattice or (10,3)-*a* structure [36–43] has Majorana Fermi surfaces, which would

be destabilized by an additional time-reversal interaction leaving an odd number of nodal lines [44, 45].

Finally, we would like to discuss the possibility to realize gapped spin liquid ground states, i.e. topological phases with ground state degeneracy. Kitaev [2] pointed out that a non-Abelian gapped topological phase would emerge from the honeycomb Kitaev model by applying a magnetic field along the [111] direction in Fig. 1(a), and an Abelian gapped Z_2 topological phase, described by the toric code [46], can be induced by introducing the bond anisotropy, i.e. breaking the three-fold symmetry of the system. The former situation is simply expected when we apply an external magnetic field to the proposed honeycomb MOFs in the same way as iridates. Concerning the latter possibility of the gapped Abelian Z_2 topological phase, realization in iridates would require an application of a uniaxial strain, which turns out to be experimentally difficult. In contrast, in MOFs, the bond anisotropy may be introduced chemically using heterogeneous organic ligands, leading to the Z_2 topological phase, as we present details in Supplemental Material. An example of possible MOF structures with heterogeneous ligands is shown in Fig. S6. Similar distorted honeycomb MOFs with heterogeneous ligands were already reported [47], so we expect that the materials proposed here could be synthesized.

Conclusion. — We discussed the possibility to realize Kitaev spin liquids in MOFs and found three advantages over inorganic materials: the suppression of undesired direct exchange interactions, the flexibility to control the parameters using a variety of possible ligands, and the natural realization of complex structures. All of these features of MOFs will pave a way towards an experimental realization of the exotic Kitaev spin liquids as the ground states, one of the holy grails in contemporary condensed matter physics.

Due to the large unit cell of MOFs, similarly to new Kitaev-dominant iridates with a longer $\text{Ir} - \text{O} - \text{O} - \text{Ir}$ superexchange [48], the energy scale of the superexchange interaction will be 10–100 K. The finite-temperature phase transition into the Kitaev spin liquid phase in the 3D case is expected at 1/100 of this energy scale [49], namely at 0.1–1 K. Although this will make the experimental studies of the Kitaev spin liquid phase below this temperature somewhat challenging, it is still possible as it is reachable with a dilution refrigerator.

Our proposal opens up many questions. We have not discussed the geometric stability of the proposed MOFs, but there is no obvious obstacle for realization of metal-oxalate frameworks with Ru^{3+} considering many reports of synthesizing metal-oxalate frameworks with various metals [11, 13, 19, 20, 34, 37–40, 43]. In fact, honeycomb MOFs with $R3c$ and $P6/mmm$ space groups, which respect a full symmetry of the honeycomb lattice, was realized with the high-spin Fe^{3+} ions [11]. We can thus naturally expect that replacement by the low-spin Ru^{3+} would not lead to any lattice distortions from the ideal

ized case [50] because of the proximity of the ionic radii, in contrast to honeycomb iridates with small monoclinic distortions [27]. It is still subtle whether a possible trigonal distortion [51], which does not break any space group symmetry, supports the formation of our proposed structure to stabilize the spin liquid states [52, 53]. Assuming the effect of the trigonal distortion of the RuO_6 octahedra in MOFs is the same as that in iridates, a recent study [27] discovered that the Kitaev term would dominate when $\angle(\text{O} - \text{Ru} - \text{O}) \sim 80^\circ$, which quite agrees with the observed values in MOFs [54]. In any case, we will need a more rigorous first-principles calculation with geometric optimization.

We thank A. Banisafar, L. E. Darago, D. E. Freedman, T. D. Harris, M. Hermanns, G. Jackeli and J. R. Long in particular for illuminating discussions. We also wish to acknowledge H. Aoki, M. Dincă, M. Gohlke, T. Hamai, D. Hirai, H. Katsura, I. Kimchi, T. Ozaki, F. Pollmann, T. Soejima, Y. Tada, H. Takagi, N. Tsuji, S. Tsuneyuki, H. Watanabe and J. Yamazaki for helpful comments. The computation in this work has been done using the facilities of the Supercomputer Center, the Institute for Solid State Physics, the University of Tokyo. The crystal data included in this work have been taken from the Cambridge Crystallographic Data Centre. M.G.Y. is supported by the Materials Education program for the future leaders in Research, Industry, and Technology (MERIT), and by JSPS. H.F. is supported by JSPS through Program for Leading Graduate Schools (ALPS). This work was supported by JSPS KAKENHI Grant Numbers JP15H02113, JP16J04752, JP17J05736, and by JSPS Strategic International Networks Program No. R2604 “TopoNet”. This research was supported in part by the National Science Foundation under Grant No. NSF PHY-1125915.

-
- [1] L. Balents, *Nature* **464**, 199 (2010).
 [2] A. Kitaev, *Ann. Phys.* **321**, 2 (2006), January Special Issue.
 [3] K. O’Brien, M. Hermanns, and S. Trebst, *Phys. Rev. B* **93**, 085101 (2016).
 [4] G. Jackeli and G. Khaliullin, *Phys. Rev. Lett.* **102**, 017205 (2009).
 [5] A. Shitade, H. Katsura, J. Kuneš, X.-L. Qi, S.-C. Zhang, and N. Nagaosa, *Phys. Rev. Lett.* **102**, 256403 (2009).
 [6] K. W. Plumb, J. P. Clancy, L. J. Sandilands, V. V. Shankar, Y. F. Hu, K. S. Burch, H.-Y. Kee, and Y.-J. Kim, *Phys. Rev. B* **90**, 041112 (2014).
 [7] Y. Yamaji, T. Suzuki, T. Yamada, S.-i. Suga, N. Kawashima, and M. Imada, *Phys. Rev. B* **93**, 174425 (2016).
 [8] I. Kimchi and Y.-Z. You, *Phys. Rev. B* **84**, 180407 (2011).
 [9] K. Kitaura, T. Sawai, T. Asada, T. Nakano, and M. Uebayasi, *Chem. Phys. Lett.* **312**, 319 (1999).
 [10] A. Weiss, E. Riegler, and C. Robl, *Z. Naturforsch.* **41b**, 1501 (1986).
 [11] C. Mathonière, C. J. Nuttall, S. G. Carling, and P. Day, *Inorg. Chem.* **35**, 1201 (1996).
 [12] B. F. Abrahams, J. Coleiro, B. F. Hoskins, and R. Robson, *Chem. Commun.*, 603 (1996).
 [13] E. Coronado, J.-R. Galán-Mascarós, C.-J. Gómez-García, J. Enslin, and P. Gütlich, *Chem. Eur. J.* **6**, 552 (2000).
 [14] B. F. Abrahams, J. Coleiro, K. Ha, B. F. Hoskins, S. D. Orchard, and R. Robson, *J. Chem. Soc., Dalton Trans.*, 1586 (2002).
 [15] T.-T. Luo, Y.-H. Liu, H.-L. Tsai, C.-C. Su, C.-H. Ueng, and K.-L. Lu, *Eur. J. Inorg. Chem.* **2004**, 4253 (2004).
 [16] G. V. Shilov, Z. K. Nikitina, N. S. Ovanesyan, S. M. Aldoshin, and V. D. Makhaev, *Russ. Chem. Bull.* **60**, 1209 (2012).
 [17] M. Atzori, S. Benmansour, G. M. Espallargas, M. Clemente-León, A. Abhervé, P. Gómez-Claramunt, E. Coronado, F. Artizzu, E. Sessini, P. Deplano, A. Serpe, M. L. Mercuri, and C. J. G. García, *Inorg. Chem.* **52**, 10031 (2013).
 [18] A. Abhervé, M. Clemente-León, E. Coronado, C. J. Gómez-García, and M. Verneret, *Inorg. Chem.* **53**, 12014 (2014).
 [19] B. Zhang, Y. Zhang, Z. Wang, D. Wang, P. J. Baker, F. L. Pratt, and D. Zhu, *Sci. Rep.* **4**, 6451 (2014).
 [20] H. Okawa, M. Sadakiyo, K. Otsubo, K. Yoneda, T. Yamada, M. Ohba, and H. Kitagawa, *Inorg. Chem.* **54**, 8529 (2015).
 [21] I.-R. Jeon, B. Negru, R. P. V. Duyne, and T. D. Harris, *J. Am. Chem. Soc.* **137**, 15699 (2015).
 [22] I. Huskić, I. V. Pekov, S. V. Krivovichev, and T. Friščić, *Sci. Adv.* **2**, e1600621 (2016).
 [23] T. Fujino, Y. Hoshino, M. Eto, Y. Yukawa, J. Fiedler, and W. Kaim, *Chem. Lett.* **32**, 274 (2003).
 [24] W. Kaim and G. K. Lahiri, *Angew. Chem., Int. Ed.* **46**, 1778 (2007).
 [25] M. J. Graham, J. M. Zadrozny, M. Shiddiq, J. S. Anderson, M. S. Fataftah, S. Hill, and D. E. Freedman, *J. Am. Chem. Soc.* **136**, 7623 (2014).
 [26] M. Fujita, K. Wakabayashi, K. Nakada, and K. Kusakabe, *J. Phys. Soc. Jpn.* **65**, 1920 (1996).
 [27] S. M. Winter, Y. Li, H. O. Jeschke, and R. Valentí, *Phys. Rev. B* **93**, 214431 (2016).
 [28] J. Chaloupka, G. Jackeli, and G. Khaliullin, *Phys. Rev. Lett.* **105**, 027204 (2010).
 [29] J. G. Rau, E. K.-H. Lee, and H.-Y. Kee, *Phys. Rev. Lett.* **112**, 077204 (2014).
 [30] T. Ozaki, *Phys. Rev. B* **67**, 155108 (2003).
 [31] W. R. Browne, R. Hage, and J. G. Vos, *Coord. Chem. Rev.* **250**, 1653 (2006).
 [32] S. Mandal and N. Surendran, *Phys. Rev. B* **79**, 024426 (2009).
 [33] T. Takayama, A. Kato, R. Dinnebier, J. Nuss, H. Kono, L. S. I. Veiga, G. Fabbris, D. Haskel, and H. Takagi, *Phys. Rev. Lett.* **114**, 077202 (2015).
 [34] B. Zhang, Y. Zhang, and D. Zhu, *Dalton Trans.* **41**, 8509 (2012).
 [35] M. Hermanns, K. O’Brien, and S. Trebst, *Phys. Rev. Lett.* **114**, 157202 (2015).
 [36] A. F. Wells, *Three-dimensional Nets and Polyhedra* (Wiley, New York, 1977).
 [37] H. Tamaki, Z. J. Zhong, N. Matsumoto, S. Kida, M. Koikawa, N. Achiwa, Y. Hashimoto, and H. Okawa,

- J. Am. Chem. Soc. **114**, 6974 (1992).
- [38] S. Decurtins, H. W. Schmalke, R. Pellaux, P. Schneuwly, and A. Hauser, *Inorg. Chem.* **35**, 1451 (1996).
- [39] E. Coronado, J. R. Galán-Mascarós, C. J. Gómez-García, and J. M. Martínez-Agudo, *Inorg. Chem.* **40**, 113 (2001).
- [40] R. Clément, S. Decurtins, M. Gruselle, and C. Train, *Monatsh. Chem.* **134**, 117 (2003).
- [41] S. Benmansour, C. Vallés-García, P. Gómez-Claramunt, G. M. Espallargas, and C. J. Gómez-García, *Inorg. Chem.* **54**, 5410 (2015).
- [42] L. E. Darago, M. L. Aubrey, C. J. Yu, M. I. Gonzalez, and J. R. Long, *J. Am. Chem. Soc.* **137**, 15703 (2015).
- [43] A. Dikhtiarenko, P. Villanueva-Delgado, R. Valiente, J. R. García, and J. Gimeno, *Polymers* **8**, 48 (2016).
- [44] M. Hermanns and S. Trebst, *Phys. Rev. B* **89**, 235102 (2014).
- [45] M. Hermanns, S. Trebst, and A. Rosch, *Phys. Rev. Lett.* **115**, 177205 (2015).
- [46] A. Kitaev, *Ann. Phys.* **303**, 2 (2003).
- [47] N. Marino, D. Armentano, G. De Munno, F. Lloret, J. Cano, and M. Julve, *Dalton Trans.* **44**, 11040 (2015).
- [48] A. Catuneanu, J. G. Rau, H.-S. Kim, and H.-Y. Kee, *Phys. Rev. B* **92**, 165108 (2015).
- [49] J. Nasu, M. Udagawa, and Y. Motome, *Phys. Rev. Lett.* **113**, 197205 (2014).
- [50] See Supplemental Material at [URL will be inserted by publisher] for the lattice distortions in 3D structures.
- [51] J. G. Rau and H.-Y. Kee, arXiv:1408.4811 [cond-mat.str-el].
- [52] L. Öhrström and K. Larsson, *Dalton Trans.* , 347 (2004).
- [53] M. Gruselle, C. Train, K. Boubekeur, P. Gredin, and N. Ovanesyan, *Coord. Chem. Rev.* **250**, 2491 (2006).
- [54] For example, the observed bond angles in various MOFs discussed in Ref. [43] range from 81° to 83° , which allows us to fine-tune the parameters by the chemical control.

Supplemental Material for “Designing Kitaev spin liquids in metal-organic frameworks”

Masahiko G. Yamada,¹ Hiroyuki Fujita,¹ and Masaki Oshikawa¹

¹*Institute for Solid State Physics, University of Tokyo, Kashiwa 277-8581, Japan.*

In this Supplemental Material, we have the following sections. Section A: the calculation details of the molecular orbitals within density functional theory (DFT), Section B: the calculated results for the molecular orbitals, Section C: the derivation of the edge states of oxalate-based ligands from the tight-binding model, Section D: the derivation of the JKT model from the microscopic model and the order estimation of the ratio of the parameters with molecular orbital diagrams for the proposed ligands, Section E: the microscopic spin model for the metal-organic frameworks with heterogeneous organic ligands, and Section F: the lattice distortions in three-dimensional structures.

Section A: PROFILES FOR THE DFT CALCULATIONS

Our analysis is based mostly on simple tight-binding models or on a fragment molecular orbital method [1] in combination with a DFT method for organic molecules. We used a first-principles electronic structure calculation code called OPENMX [2] for the DFT calculations. In OPENMX, one-particle wave functions are expressed by the linear combination of pseudoatomic basis functions (LCPAO) and the norm-conserving pseudopotentials are used. We used the generalized gradient approximation represented by Perdew, Burke and Ernzerhof (GGA-PBE) [3] for the exchange-correlation potential. A self-consistent loop was iterated until the energy was relaxed with the error of 10^{-10} Hartree. The geometric optimization of internal coordinates was also iterated until the force became smaller than 10^{-4} Hartree/Bohr with a constraint on the molecules to be completely planar.

In order to calculate the molecular orbitals of the proposed ionic ligands, we used an energy cutoff of 500 Ry for the numerical integrations and the solution of the Poisson equation using the fast Fourier transformation algorithm. As basis functions, $2s$, $2p$, $3s$, $3p$, and $3d$ -orbitals for C, N, O, $3s$, $3p$, $3d$, $4s$, and $4p$ -orbitals for S, and $1s$, $2s$, $2p$ -orbitals for H were employed. In OPENMX, the excess charge of the ionic state of the ligands is compensated by a uniform background electronic charge with an opposite sign, which is an artificial approximation for the numerical reason. All the calculations are done without including a spin-orbit coupling or spin polarization. The results of these calculations are included mostly in this Supplemental Material.

In addition, the crystal data for Fig. S1 was taken from the Cambridge Structural Database [4] in order to show the hyperhoneycomb structure.

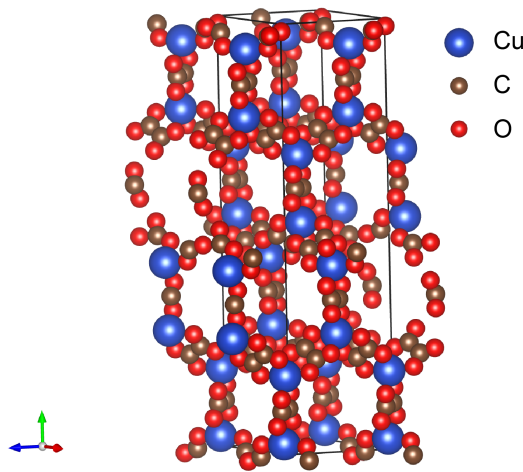


FIG. S1. Hyperhoneycomb structure of a metal-oxalate framework. This structure is included in [5] (Cu: blue, C: brown, O: red), reconstructed from the crystal data taken from CSD-KEDJAG in the Cambridge Structural Database [4]. The auxiliary structure other than metal ions and oxalate ions are omitted for simplicity.

TABLE I. Parameters for each molecule estimated from DFT calculations.

	molecule	formula	$t_{\pi\pi}$ (eV)	$t_{\pi^*\pi^*}$ (eV)	$V_{\pi^*} - V_{\pi}$ (eV)
(a)	oxalate	$(\text{C}_2\text{O}_4)^{2-}$	0.153	1.631	6.474
(b)	$(\text{C}_4\text{N}_6\text{H}_4)^{2-}$		0.208	1.501	4.107
(c)	tetraaminooxalate	$(\text{C}_2\text{N}_4\text{H}_4)^{2-}$	0.215	1.526	5.091
(d)	tetrathiooxalate	$(\text{C}_2\text{S}_4)^{2-}$	0.238	1.201	3.012

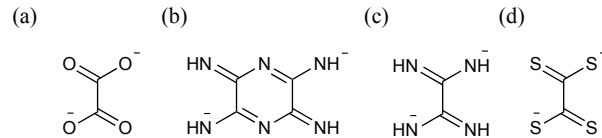


FIG. S2. Structure formulae of the proposed ligands listed in Table I. (a) Oxalate, an ionized form of **1** with $E = \text{O}$ in Fig. 2(a) in the main text. (b) $(\text{C}_4\text{N}_6\text{H}_4)^{2-}$, an ionized form of **3** in Fig. 2(a) in the main text. (c) Tetraaminooxalate, an ionized form of **1** with $E = \text{NH}$ in Fig. 2(a) in the main text. (d) Tetrathiooxalate, an ionized form of **1** with $E = \text{S}$ in Fig. 2(a) in the main text.

Section B: CALCULATED MOLECULAR ORBITALS

Using the conditions for OPENMX [2] described in Section A, we calculated the molecular orbitals near the Fermi energy for three oxalate-based ligands (**1** with $E = \text{O}$, NH , S in Fig. 2(a) in the main text, corresponding to (a), (c), (d) in Fig. S2, respectively) and one tetraaminopyrazine-based ligand (**3** in Fig. 2(a) in the main text, corresponding to (b) in Fig. S2), based on DFT. After the geometric optimization, all the molecules are relaxed to have a D_{2h} symmetry.

In the case of oxalate shown in Fig. S2(a), the π -conjugated highest occupied molecular orbitals (HOMOs) localized along the boundaries consist mostly of oxygen p_z -orbitals and are well-separated from each other. We can thus easily express these orbitals by linear combinations of upper-half and lower-half “fragment molecular orbitals” (fMOs) localized along each boundary. (Here we regard the y -direction in Fig. S3 as the vertical direction, viewing from the z -direction.) The calculated HOMO, HOMO-1 and HOMO-2 are σ -orbitals with oxygen s -orbitals and thus ignored here, because they cannot hybridize with the Ru t_{2g} -orbitals. (HOMO- n refers to the molecular orbital n -th in the energy below the highest occupied one.) The calculated HOMO-3 shown in Fig. S3(a) (resp. HOMO-4 shown in Fig. S3(b)) is an antisymmetric (resp. symmetric) π -conjugated HOMO (π -HOMO in short) of oxalate and we define the creation operator for this state as a^\dagger (resp. b^\dagger). Actually, we could decompose this orbital by $a^\dagger = (u^\dagger - l^\dagger)/\sqrt{2}$ (resp. $b^\dagger = (u^\dagger + l^\dagger)/\sqrt{2}$) using the upper-half fMO u^\dagger shown in Fig. S3(c) and the lower-half fMO l^\dagger shown in Fig. S3(d). If we regard the potential energy of the two fMOs as V_π and define a hopping $-t_{\pi\pi}$ between these two orbitals, then it can easily be concluded that HOMOs $a^\dagger(b^\dagger) = (u^\dagger \mp l^\dagger)/\sqrt{2}$ have an energy of $V_\pi \pm t_{\pi\pi}$, respectively. From the calculated energy of HOMO-3 and HOMO-4, we can estimate the value of V_π and $t_{\pi\pi}$. Similarly, we can decompose the π -conjugated lowest unoccupied molecular orbitals (LUMOs) (LUMO and LUMO+1 shown in Fig. S3(e) and Fig. S3(f), respectively, in the case of oxalate) into two pieces and estimate the value of the potential energy V_{π^*} and the hopping $t_{\pi^*\pi^*}$ for these LUMOs. (LUMO+ n refers to the molecular orbital n -th in the energy above the lowest unoccupied one.) In Table I, we summarize the value of $t_{\pi\pi}$, $t_{\pi^*\pi^*}$, and $V_{\pi^*} - V_\pi$ obtained in this way for each ligand molecule. The absolute values of the potential energy V_π and V_{π^*} obtained in the present calculation are not quite meaningful if molecules are included in actual MOFs. However, the difference $V_{\pi^*} - V_\pi$ is physical and thus is listed in Table I.

In the case of $(\text{C}_4\text{N}_6\text{H}_4)^{2-}$ shown in Fig. S2(b), the two π -HOMOs shown in Fig. S3(g) and Fig. S3(h) are just below the Fermi energy even in the vacuum and there is no irrelevant σ -HOMO between the Fermi energy and these π -HOMOs. In the case of tetraaminooxalate shown in Fig. S2(c), the two π -HOMOs shown in Fig. S3(i) and Fig. S3(j) have the same property.

Since tetrathiooxalate shown in Fig. S2(d) might be able to coordinate almost octahedrally to the metal ion M^{3+} , ($M = \text{Ru}$, Os , etc.) i.e. $\angle(\text{S} - M - \text{S}) \sim 90^\circ$, the replacement of $E = \text{O}$ by S could possibly lead to a better ligand field [6] for the Jackeli-Khaliullin mechanism [7], in terms of coupling to the $M = \text{Ru}$ t_{2g} -orbitals. On the other hand, the DFT calculation suggests that the π -HOMOs shown in Fig. S3(k) and Fig. S3(l) are not as degenerate in tetrathiooxalate as in oxalate. This is rather disadvantageous for the cancellation of the Heisenberg interaction due

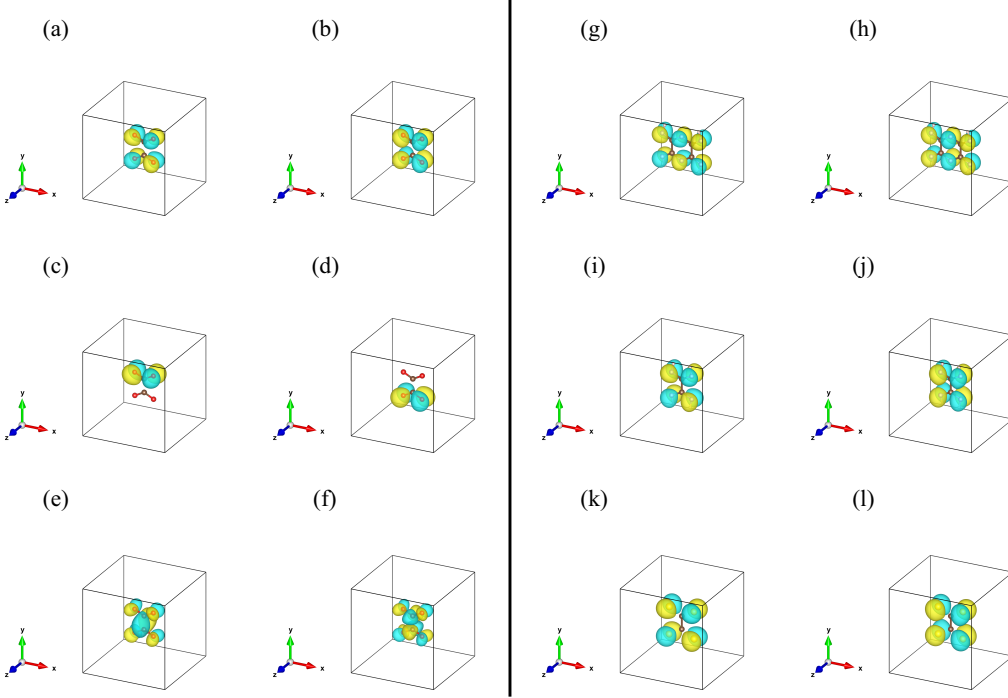


FIG. S3. Molecular orbitals of ligands. (a) Antisymmetric HOMO-3 of oxalate created by $a^\dagger = (u^\dagger - l^\dagger)/\sqrt{2}$ with an energy $E = -2.089$ eV. (b) Symmetric HOMO-4 of oxalate created by $b^\dagger = (u^\dagger + l^\dagger)/\sqrt{2}$ with $E = -2.396$ eV. (c) Upper-half fMO of oxalate created by u^\dagger . (d) Lower-half fMO of oxalate created by l^\dagger . (e) Symmetric LUMO of oxalate with $E = 2.6$ eV (criterion). (f) Antisymmetric LUMO+1 of oxalate with $E = 5.862$ eV. (g) Antisymmetric HOMO of $(C_4N_6H_4)^{2-}$ with $E = -1.418$ eV. (h) Symmetric HOMO-1 of $(C_4N_6H_4)^{2-}$ with $E = -1.833$ eV. (i) Antisymmetric HOMO of tetraaminoxalate with $E = -1.531$ eV. (j) Symmetric HOMO-1 of tetraaminoxalate with $E = -1.961$ eV. (k) Antisymmetric HOMO-2 of tetrathiooxalate with $E = -1.497$ eV. (l) Symmetric HOMO-5 of tetrathiooxalate with $E = -1.973$ eV. In each panel, yellow and blue bubbles represent plus and minus isosurfaces, respectively (C: brown, O: red, H: white, N: light blue, S: yellow for atoms).

to the Jackeli-Khaliullin mechanism, as we discussed in the main text. By comparing Table I and Fig. S3, we can see that $t_{\pi\pi}$ grows ($O < NH < S$) as the wavefunction around chalcogen (or NH) expands.

Section C: EDGE STATES FROM THE TIGHT-BINDING MODEL

In order to understand the physical origin of the nearly-degenerate π -HOMO states, which are important for the realization of the Jackeli-Khaliullin mechanism, we discuss a tight-binding model (or LCAO (linear combination of atomic orbitals) Hückel approximation) for the ligand molecules. As an example, here we discuss the simplest case of oxalate as the ligand molecule. We consider the six $2p_z$ -orbitals of C and O atoms of oxalate. Assuming the planar structure and D_{2h} symmetry of oxalate, the tight-binding hopping Hamiltonian in the first-quantized form should be written in the following 6×6 matrix.

$$H_{\text{ox}} = \begin{pmatrix} 0 & -t'_{\text{OO}} & -t_{\text{OC}} & -t''_{\text{OO}} & -t'''_{\text{OO}} & -t'_{\text{OC}} \\ -t'_{\text{OO}} & 0 & -t_{\text{OC}} & -t'''_{\text{OO}} & -t''_{\text{OO}} & -t'_{\text{OC}} \\ -t_{\text{OC}} & -t_{\text{OC}} & \Delta & -t'_{\text{OC}} & -t'_{\text{OC}} & -t_{\text{CC}} \\ -t''_{\text{OO}} & -t'''_{\text{OO}} & -t'_{\text{OC}} & 0 & -t'_{\text{OO}} & -t_{\text{OC}} \\ -t'''_{\text{OO}} & -t''_{\text{OO}} & -t'_{\text{OC}} & -t'_{\text{OO}} & 0 & -t_{\text{OC}} \\ -t'_{\text{OC}} & -t'_{\text{OC}} & -t_{\text{CC}} & -t_{\text{OC}} & -t_{\text{OC}} & \Delta \end{pmatrix}, \quad (1)$$

where Δ is the difference in the potential energy between O and C, the $2p_z$ -orbital of each atom is numbered and the real-valued hopping parameters are defined as shown in Fig. S4(a) and Fig. S4(b).

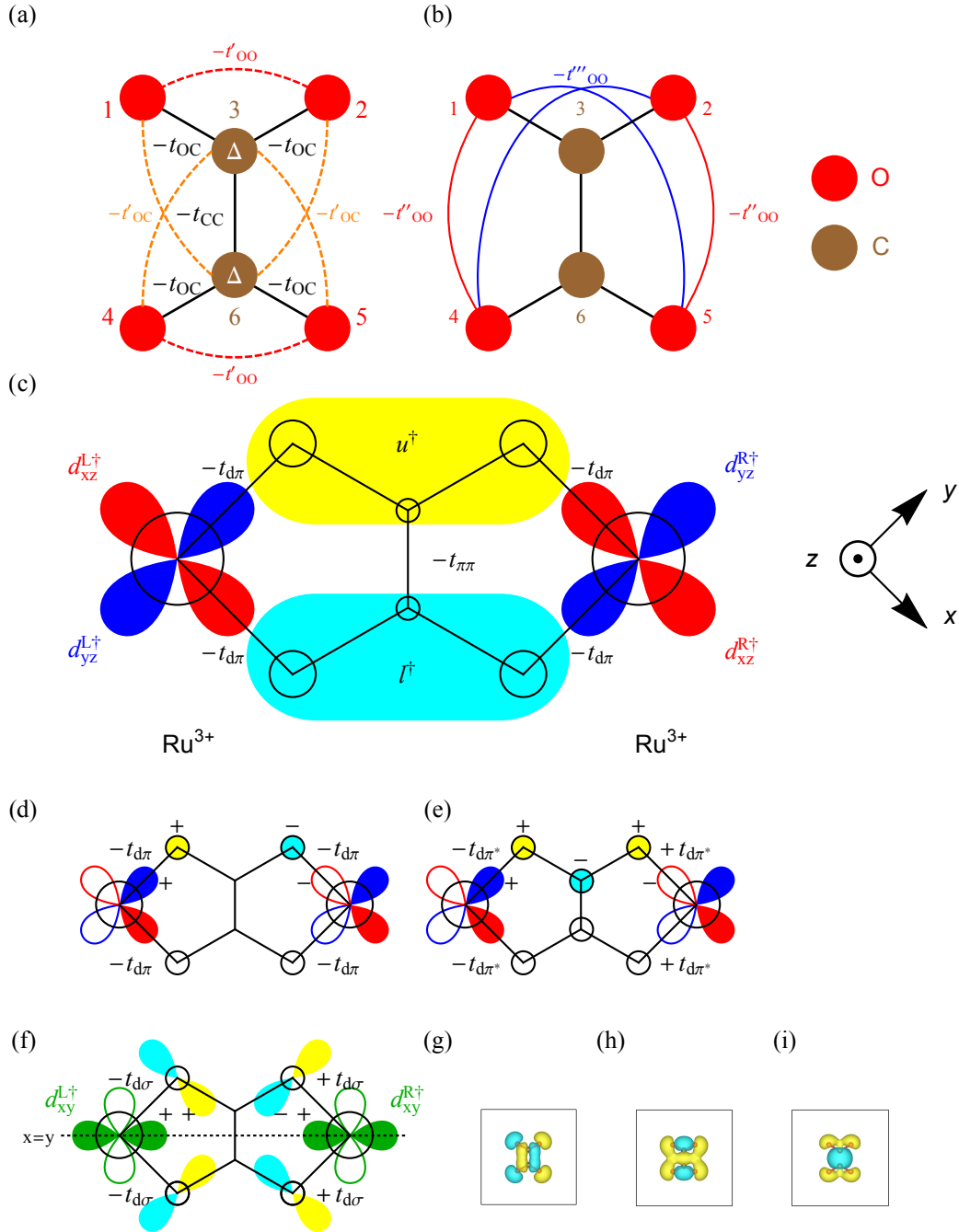


FIG. S4. Tight-binding model for superexchange interactions. (a) Tight-binding model for the oxalate ion with NN and 2NN interactions. (b) 3NN and 4NN interactions which break the degeneracy. (c) Tight-binding model for the superexchange pathways between the Ru t_{2g} -orbitals. (d) Upper-half superexchange pathway for the π -HOMOs of oxalate. (e) Upper-half superexchange pathway for the π -LUMOs of oxalate. The signs of the contribution to the spin model are different between the two because the superposition coefficients of the oxygen p_z -orbitals are different in the DFT calculations (compare Fig. S3(a) and Fig. S3(b) to Fig. S3(e) and Fig. S3(f)). (f) Possible superexchange pathway between the Ru d_{xy} -orbitals. (g) HOMO-8 (deep σ -orbital) of oxalate with $E = -6.150$ eV when viewed from the z -direction, which has the symmetry to hybridize to the Ru d_{xy} -orbitals. (h) HOMO-10 with $E = -6.628$ eV. (i) HOMO-12 with $E = -10.40$ eV.

First, we ignore the further-neighbor interactions by setting $t'_{\text{OO}} = t''_{\text{OO}} = t'''_{\text{OO}} = t'_{\text{OC}} = 0$, and consider only the potential energy and the nearest-neighbor (NN) interactions. In this case, by diagonalizing the Hamiltonian, we get one pair of positive-energy modes, another pair of negative-energy modes, and two degenerate zero-energy modes, $(1, -1, 0, 0, 0)/\sqrt{2}$ and $(0, 0, 0, 1, -1, 0)/\sqrt{2}$ as energy eigenstates. In the present material, π -conjugated molecular orbitals are $2/3$ -filled, and thus these degenerate pairs of states correspond to π -HOMOs. Namely, the double degeneracy of the π -HOMO states is exact in the limit where only NN hoppings are allowed. These two degenerate zero modes are similar to the $k = \pi$ zigzag edge modes of graphene, and thereby localized on the O atoms. Therefore, the (nearly) degenerate π -HOMOs can be physically interpreted as “edge states” along the upper and lower sides of the ligand molecule.

Let us now discuss the effects of further-neighbor hoppings. We find that, because of the symmetry of the molecule, the second-nearest-neighbor (2NN) interactions t'_{OO} and t'_{OC} do not lift the degeneracy of π -HOMOs even though they may shift their overall energy. Thus, the degeneracy is only lifted by introducing the third-nearest-neighbor (3NN) hopping t''_{OO} or the fourth-nearest-neighbor (4NN) hopping t'''_{OO} shown in Fig. S4(b) with an energy split of $2t_{\pi\pi} = 2(t''_{\text{OO}} - t'''_{\text{OO}})$. Therefore, in terms of the tight-binding model, we can identify the effective tunneling matrix element $t_{\pi\pi}$ between the two π -HOMOs with $t''_{\text{OO}} - t'''_{\text{OO}}$. It is naturally expected that this value would be smaller than the NN and 2NN interactions, as they involve longer-range hoppings. From the DFT calculation, we obtain $t_{\pi\pi} = 0.153$ eV. The smallness of this value, compared to the other energy scale $V_{\pi^*} - V_{\pi} = 6.474$ eV, indeed reflects this mechanism.

Since the 4NN hopping t'''_{OO} would be suppressed more strongly than the 3NN one t''_{OO} , we can approximately identify $t''_{\text{OO}} \sim t_{\pi\pi} = 0.153$ eV. We note that, even this small value of $t_{\pi\pi}$ may be an overestimation in our calculation done for the ligand molecule in vacuum; in the actual metal-organic frameworks, there is an electron density from the Ru atoms between the upper and lower oxygens, which would screen the hopping between the oxygens and thus suppress t''_{OO} . The analysis here applies to all of the oxalate family; the nearly-degenerate π -HOMOs can be similarly understood as “edge states,” which are exactly degenerate within the tight-binding approximation with the NN and 2NN hoppings.

Finally, we comment on the tetraaminopyrazine case in the qualitative level. In the analysis similar to the oxalate case, we find two edge states also for this ligand molecule. However, unlike the oxalate case, these states are split due to the incomplete degeneracy of the renormalized potential energy of the three N atoms, or the discrepancy between the 2NN interactions between the N and C atoms. As a consequence, $t_{\pi\pi}$ should be larger in the tetraaminopyrazine case than in the oxalate case, which agrees with the DFT results shown in Table I. We also note that there is no reason to expect near-degeneracy in $\text{d}(\text{hbq})^{2-}$ or $X_2\text{An}^{2-}$ ($\text{d}(\text{hbq}) = 2,5\text{-dihydroxy-1,4-benzoquinone}$, $X = \text{Cl, Br, etc.}$ and $\text{An} = \text{anilate}$) and the difference between these ligands and the tetraaminopyrazine-based ligand comes from the substantial potential difference between the chalcogen p_z -orbital and the C p_z -orbital.

Section D: DERIVATION OF THE JKIΓ MODEL

We construct a microscopic model for the superexchange between the Ru t_{2g} -orbitals via the planar organic ligand in the xy plane using the fMO method. We mostly consider superexchange pathways through the π -conjugated system, i.e. p_z -orbitals. Actually, the symmetry allows hybridization between the Ru t_{2g} -orbitals and the p_x or p_y -orbitals of chalcogens (or nitrogen) and they can form σ -HOMOs or σ^* -LUMOs of the organic ligand. However, the DFT results suggest that such orbitals will not form any superexchange pathways near the Fermi energy for oxalate and tetraaminopyrazine, and there only remains σ -HOMOs or σ^* -LUMOs with s -orbitals (or the orbitals with the same symmetry when viewed from Ru) on oxygens (in the case of oxalate), which cannot be hybridized with the Ru t_{2g} -orbitals near the Fermi level. For oxalate, the first σ -HOMO that contributes to the superexchange interaction is HOMO-8 far below the Fermi energy and we mostly consider the contribution of this orbital from σ -HOMOs.

For π -HOMOs, we divide the π -conjugated molecular orbital of the organic ligand into the upper-half fMO with a creation operator u^\dagger and the lower-half fMO with a creation operator l^\dagger , as shown in Fig. S4(c). If we define a real-valued hopping amplitude $-t_{\pi\pi}$ between these two fMOs, it can easily be concluded that HOMOs $(u^\dagger \pm l^\dagger)/\sqrt{2}$ would be split with the energy of $V_{\pi} \mp t_{\pi\pi}$, respectively, assuming the potential energy of the π -HOMOs as V_{π} . If we regard u^\dagger and l^\dagger as p_z -orbitals of two oxygens between Ir^{4+} in iridates [7], we can conclude that the superexchange interaction would be completely Kitaev-type by the Jackeli-Khaliullin mechanism when $t_{\pi\pi} = 0$. It is known that the Kitaev interaction comes from the off-diagonal hopping between t_{2g} -orbitals, such as between d_{xz} and d_{yz} , while the Heisenberg interaction mainly comes from the diagonal part. The diagonal element of the hopping matrix always needs the hopping between u^\dagger and l^\dagger somewhere in the superexchange pathway, so it must be important to newly include the effect of $t_{\pi\pi}$ to estimate the interactions other than the Kitaev term. By comparing with the results

in the previous section, we can regard the u^\dagger state as $(1, -1, 0, 0, 0)/\sqrt{2}$ and the l^\dagger state as $(0, 0, 0, 1, -1, 0)/\sqrt{2}$ in oxalate. We note that the present fMO analysis does not require the near-degeneracy of π -HOMOs, although the near-degeneracy is advantageous for the Jackeli-Khaliullin mechanism. In fact, in the explicit derivation of the effective model, we can see how the near-degeneracy is important for the suppression of the Heisenberg term.

The model Hamiltonian in the second-quantized form is

$$H = -t_{d\pi}(u^\dagger d_{yz}^L + l^\dagger d_{xz}^L + u^\dagger d_{xz}^R + l^\dagger d_{yz}^R + h.c.) + V_\pi(u^\dagger u + l^\dagger l) - t_{\pi\pi}(u^\dagger l + l^\dagger u), \quad (2)$$

where $-t_{d\pi}$ is a real-valued hopping element between the Ru t_{2g} -orbitals and the fMO, V_π is a potential energy which electrons from Ru feel on the fMOs, and d_i^L (resp. d_i^R) is the annihilation operator of an electron on the Ru d_i -orbital on the left (resp. right) side in Fig. S4(c).

We define $b^\dagger = (u^\dagger + l^\dagger)/\sqrt{2}$ and $a^\dagger = (u^\dagger - l^\dagger)/\sqrt{2}$ to diagonalize the $t_{\pi\pi}$ term,

$$H = -\frac{t_{d\pi}}{\sqrt{2}}[(a^\dagger + b^\dagger)d_{yz}^L + (b^\dagger - a^\dagger)d_{xz}^L + (a^\dagger + b^\dagger)d_{xz}^R + (b^\dagger - a^\dagger)d_{yz}^R + h.c.] + (V_\pi + t_{\pi\pi})a^\dagger a + (V_\pi - t_{\pi\pi})b^\dagger b. \quad (3)$$

Then, we get an effective hopping matrix via π -HOMOs H_{dd}^π between the Ru d -orbitals from the second-order perturbation in $t_{d\pi}/|V_\pi \pm t_{\pi\pi}|$ by integrating out the b and a states.

$$H_{dd}^\pi = -\frac{t_{d\pi}^2 t_{\pi\pi}}{V_\pi^2 - t_{\pi\pi}^2}(d_{yz}^L d_{yz}^R + d_{xz}^L d_{xz}^R) - \frac{t_{d\pi}^2 V_\pi}{V_\pi^2 - t_{\pi\pi}^2}(d_{yz}^L d_{xz}^R + d_{xz}^L d_{yz}^R) + h.c. \quad (4)$$

We can repeat a similar calculation to derive the hopping matrix via the π^* -LUMOs of the organic ligand. If we define a potential energy V_{π^*} for the LUMOs, a real-valued hopping $-t_{\pi^*\pi^*}$ between the LUMOs and a real-valued hopping $-t_{d\pi^*}$ between the Ru t_{2g} -orbitals and the LUMO, we get an effective hopping matrix $H_{dd}^{\pi^*}$ as

$$H_{dd}^{\pi^*} = \frac{t_{d\pi^*}^2 t_{\pi^*\pi^*}}{V_{\pi^*}^2 - t_{\pi^*\pi^*}^2}(d_{yz}^L d_{yz}^R + d_{xz}^L d_{xz}^R) + \frac{t_{d\pi^*}^2 V_{\pi^*}}{V_{\pi^*}^2 - t_{\pi^*\pi^*}^2}(d_{yz}^L d_{xz}^R + d_{xz}^L d_{yz}^R) + h.c. \quad (5)$$

We have to note that the HOMOs and the LUMOs contribute to the effective hopping with different signs due to the difference in the superposition coefficients of the oxygen p_z -orbitals (see Fig. S4(d) for the HOMOs and Fig. S4(e) for the LUMOs). In addition, we consider σ -HOMO (HOMO-8 in oxalate) with a potential energy V_σ . The symmetry only allows the hopping $-t_{d\sigma}$ between the σ -HOMO and the Ru d_{xy} -orbital as shown in Fig. S4(f), and HOMO-8 shown in Fig. S4(g) actually possesses this property. We have to note that this energy eigenstate orbital is symmetric against $x = y$, and anti-symmetric HOMO-7 does not contribute to the superexchange between the Ru d_{xy} -orbitals.

$$H_{dd}^\sigma = \frac{(2t_{d\sigma})^2}{V_\sigma}(d_{xy}^L d_{xy}^R) + h.c. \quad (6)$$

The coefficient 2 comes from the symmetry against $x = y$ of the σ -HOMO. Combining these three contributions and following Ref. [8], we estimate an effective hopping matrix H_{dd}^{eff} between the Ru d -orbitals [9].

$$H_{dd}^{\text{eff}} = H_{dd}^\pi + H_{dd}^{\pi^*} + H_{dd}^\sigma = -t_1(d_{yz}^L d_{yz}^R + d_{xz}^L d_{xz}^R) - t_2(d_{yz}^L d_{xz}^R + d_{xz}^L d_{yz}^R) - t_3 d_{xy}^L d_{xy}^R + h.c., \quad (7)$$

$$t_1 = \frac{t_{d\pi}^2 t_{\pi\pi}}{V_\pi^2 - t_{\pi\pi}^2} - \frac{t_{d\pi^*}^2 t_{\pi^*\pi^*}}{V_{\pi^*}^2 - t_{\pi^*\pi^*}^2}, \quad (8)$$

$$t_2 = \frac{t_{d\pi}^2 V_\pi}{V_\pi^2 - t_{\pi\pi}^2} - \frac{t_{d\pi^*}^2 V_{\pi^*}}{V_{\pi^*}^2 - t_{\pi^*\pi^*}^2}, \quad (9)$$

$$t_3 = -\frac{4t_{d\sigma}^2}{V_\sigma} + \dots \quad (10)$$

Of course, $V_\pi < 0$ and $V_{\pi^*} > 0$ (while $t_{\pi\pi} > 0$ and $t_{\pi^*\pi^*} > 0$), so the π -HOMOs and the π^* -LUMOs contribute to the diagonal hopping t_1 with the opposite sign and the off-diagonal hopping t_2 with the same sign, which makes $|t_1|/|t_2|$ even smaller.

Therefore, by mapping the electron hopping matrix to the $J_{\text{eff}} = 1/2$ spin model by the second-order perturbation in t_i , we actually get the JKG model for the bond in the xy -plane, which is defined in Eq. (3) in the main text. A similar analysis is possible for bonds in the other directions and we can construct a whole JKG model for both two-dimensional (2D) and three-dimensional (3D) lattices. We note that in chiral 3D tricoordinated lattices the parity symmetry is explicitly broken and we cannot ignore Dzyaloshinskii-Moriya interactions. Assuming zero crystal field

splitting for the Ru t_{2g} -orbitals and ideal octahedral coordination, the parameters for the JKT model will be the following [8].

$$J = \frac{4\mathbb{A}}{9}(2t_1 + t_3)^2 - \frac{16\mathbb{B}}{9}(t_1 - t_3)^2, \quad (11)$$

$$K = \frac{8\mathbb{B}}{3}[(t_1 - t_3)^2 - 3t_2^2], \quad (12)$$

$$\Gamma = \frac{16\mathbb{B}}{3}t_2(t_1 - t_3), \quad (13)$$

where the parameters \mathbb{A} and \mathbb{B} can be expressed in terms with a Hund coupling J_H , a spin-orbit coupling λ , and a Hubbard term U for Ru³⁺ in [8] as follows.

$$\mathbb{A} = -\frac{1}{3} \left[\frac{J_H + 3(U + 3\lambda)}{6J_H^2 - U(U + 3\lambda) + J_H(U + 4\lambda)} \right], \quad (14)$$

$$\mathbb{B} = \frac{4}{3} \left[\frac{(3J_H - U - 3\lambda)}{(6J_H - 2U - 3\lambda)} \eta \right], \quad (15)$$

$$\eta = \frac{J_H}{6J_H^2 - J_H(8U + 17\lambda) + (2U + 3\lambda)(U + 3\lambda)}. \quad (16)$$

Then, the literature [8] estimates these parameters [10] for Ru³⁺ as $\mathbb{A} \sim 0.6 \text{ eV}^{-1}$ and $\mathbb{B} \sim 0.05 \text{ eV}^{-1}$. If we only consider the superexchange pathways through π -HOMOs (i.e. $t_3 \sim 0$), from the relations $t_1/t_2 = t_{\pi\pi}/V_\pi$ and $\mathbb{B}/\mathbb{A} \sim 1/10$, we can conclude that, if $|t_{\pi\pi}|/|V_\pi| \sim 1/10$ for two almost degenerate HOMOs, the superexchange interaction via these HOMOs should be Kitaev-dominant, i.e. $J/|K| \sim |\Gamma|/|K| \sim 1/10$. Thus, we have shown that $|t_{\pi\pi}|/|V_\pi|$ actually controls the parameters of the JKT model as expected. Next, if we consider the contribution from the π^* -LUMOs, then

$$\frac{t_{d\pi}^2 t_{\pi\pi}}{V_\pi^2} \gtrsim \frac{t_{d\pi^*}^2 t_{\pi^*\pi^*}}{V_{\pi^*}^2} \quad (17)$$

must be held in order not to change the order of $|t_1|/|t_2|$. We can roughly estimate $t_{d\pi^*}/t_{d\pi}$ as follows. If we assume only the Ru $4d_{yz}$ -orbital $|\psi_{4d_{yz}}\rangle$ and the neighboring O $2p_z$ -orbital $|\psi_{2p_z}\rangle$ contribute to the hopping element, using the real-valued LCAO coefficient c_π (resp. c_{π^*}) of the the neighboring O $2p_z$ -orbital for the HOMO (resp. LUMO), we can define a hopping element $-t_{dp} = \langle \psi_{2p_z} | H_{\text{LCAO}} | \psi_{4d_{yz}} \rangle$, where H_{LCAO} is a hopping Hamiltonian in the LCAO approximation. Then,

$$\frac{-t_{d\pi^*}}{-t_{d\pi}} = \frac{-c_{\pi^*} t_{dp}}{-c_\pi t_{dp}} = \frac{c_{\pi^*}}{c_\pi}. \quad (18)$$

Using this relation, we can estimate the $t_{d\pi^*}/t_{d\pi}$ for oxalate from the LCAO coefficients calculated by OPENMX, assuming the almost orthogonality of the pseudoatomic orbitals, as

$$\frac{t_{d\pi^*}}{t_{d\pi}} = \frac{c_{\pi^*}}{c_\pi} = \frac{\sqrt{2} \cdot 0.3063}{\sqrt{2} \cdot 0.4972} = 0.6159. \quad (19)$$

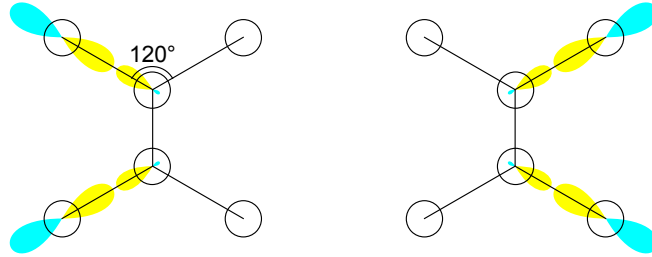


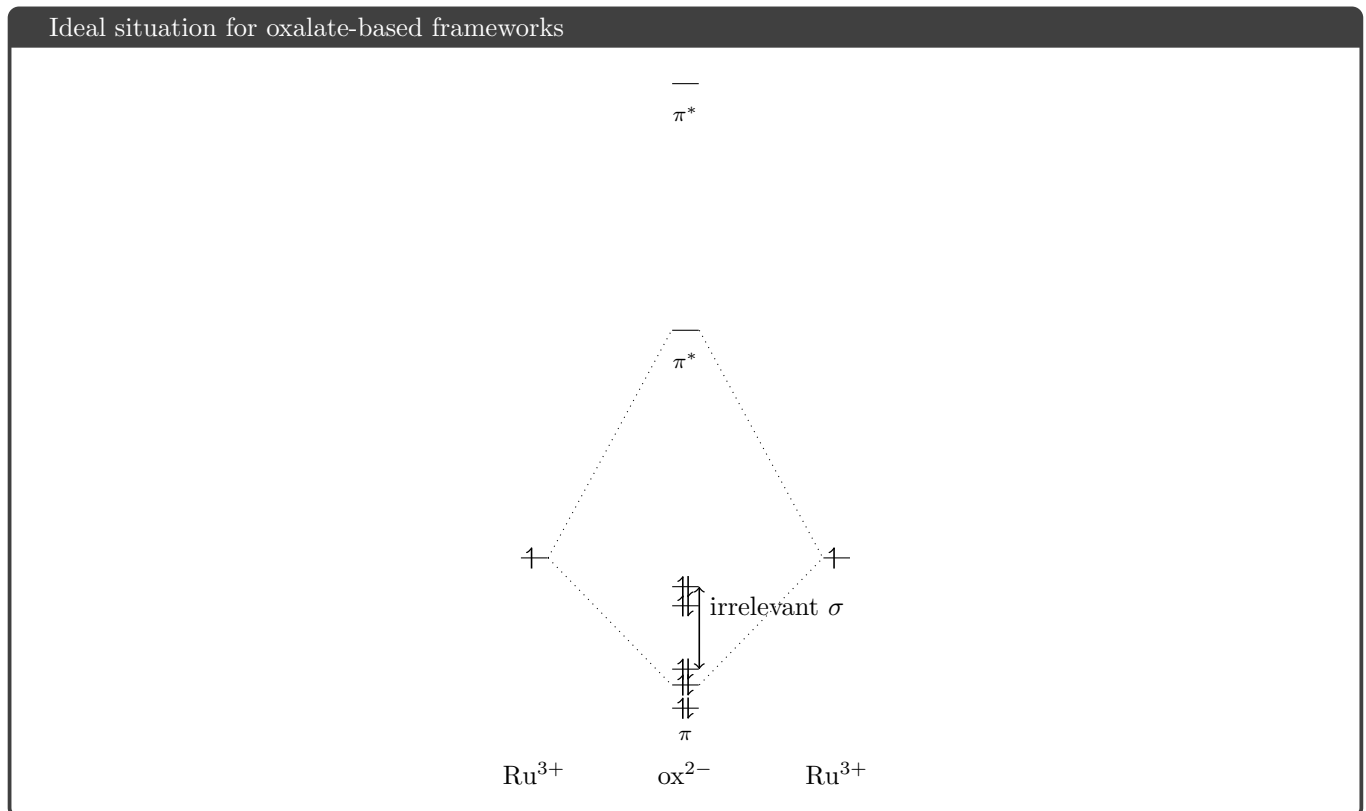
FIG. S5. Two almost degenerate σ -orbitals localized along the left and right edges. They consist of the O- p_x or p_y orbitals and the C- sp^2 hybridized orbitals.

Finally, we estimate the possible contribution to t_3 from the localized σ -orbitals. This contribution to t_3 should be smaller than the dominant contribution from delocalized π -orbitals to t_2 because the σ -orbitals form covalent bonds and the paired electrons are localized on those bonds, i.e. a charge gap is opened for these localized valence bonds. However, there is still a possibility that the magnitude of t_3 is comparable to that of t_1 , so we made a crude estimation for this contribution. As we explained above, σ -HOMOs do not contribute to the hopping near the Fermi level, so, as the first approximation, we only consider the effects of the deep levels, HOMO-8, HOMO-10, and HOMO-12 shown in Fig. S4(g), (h) and (i), respectively, with $|V_\sigma| > |V_\pi|$. These orbitals can contribute only to t_3 due to the completely planar structure of the molecule, and their contributions with different signs almost cancel out. This fact can be understood in a way similar to the earlier analysis of the degenerate π -HOMOs. From the viewpoint of localized valence bonds, two σ -orbitals localized along the left and right edge shown in Fig. S5 are almost orthogonal and degenerate assuming the 120 degrees bonding around C and the complete degeneracy of the C- sp^2 hybridized orbitals. If these orbitals are completely degenerate and localized along the edges, they do not provide any superexchange pathways. In the language of molecular orbitals, the contributions from σ -HOMOs created by the linear combination of these two edge states will be cancelled out. In the same way, we can naturally expect that the superexchange contributions from nearly degenerate HOMO-8, HOMO-10, and HOMO-12 are rather destructive, even if the degeneracy of the edge state is not perfect. The relative values of $t_{d\sigma n}$ for HOMO- n can be estimated in the same way as $t_{d\pi}$ as follows.

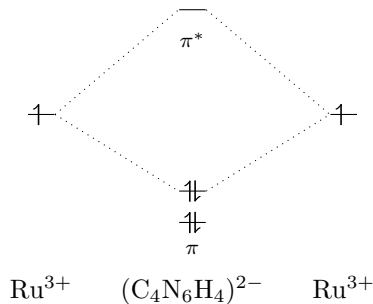
$$\frac{t_3}{t_2} = \left(-\frac{4t_{d\sigma 8}^2}{V_{\sigma 8}} + \frac{4t_{d\sigma 10}^2}{V_{\sigma 10}} + \frac{4t_{d\sigma 12}^2}{V_{\sigma 12}} \right) / t_2 \sim -0.196, \quad (20)$$

$$\frac{t_{d\sigma 8}}{t_{d\pi}} = \frac{0.4018}{\sqrt{2} \cdot 0.4972} = 0.5714, \quad \frac{t_{d\sigma 10}}{t_{d\pi}} = \frac{0.2398}{\sqrt{2} \cdot 0.4972} = 0.3410, \quad \frac{t_{d\sigma 12}}{t_{d\pi}} = \frac{0.2149}{\sqrt{2} \cdot 0.4972} = 0.3056. \quad (21)$$

From these values we can estimate $t_3/t_2 \sim -0.196$ as written in the main text. Therefore, we can conclude for oxalate that if $|t_{\pi\pi}|/|V_\pi| \sim 1/10$, $|V_\pi|/|V_{\pi^*}| \sim 1/2$ and the destructive interference in the σ -orbitals works, the interaction should be Kitaev-dominant even if we consider contributions other than the π -HOMOs. Then, the ideal situation for the Kitaev-dominant interaction can be depicted schematically as follows (ox $^{2-}$ is oxalate).



Ideal situation for tetraaminopyrazine-based frameworks



To achieve every condition, the energy level of the Ru t_{2g} -orbitals should sit in the right position between the HOMOs and the LUMOs of the proposed oxalate-based or tetraaminopyrazine-based ligands. It will be interesting to carry out more accurate analysis of these materials to see whether the dominance of the Kitaev interaction is maintained.

Section E: BOND ANISOTROPY

Here we discuss MOFs with heterogeneous organic ligands, as proposed in the section *Designing a Variety of Kitaev Spin Liquids* in the main text. The heterogeneous organic ligands could arrange themselves into an MOF with different ligand molecules depending on the orientation of the bond, as shown in Fig. S6. This will naturally lead to the effective spin Hamiltonian with bond anisotropy, namely the interaction strength depending on the bond orientation. In the following discussion, for simplicity, we ignore the Γ term of the JKT model and assume only the Kitaev-Heisenberg interaction with a bond anisotropy. The effective spin Hamiltonian on the honeycomb lattice is then given by

$$H = \sum_{\langle ij \rangle \in \alpha\beta(\gamma)} [J_\gamma \mathbf{S}_i \cdot \mathbf{S}_j - |K_\gamma| S_i^\gamma S_j^\gamma], \quad (22)$$

where $K_\gamma < 0$ is the ferromagnetic Kitaev term and J_γ is the antiferromagnetic Heisenberg term for each type of bonds as shown in Fig. S6. $\alpha, \beta, \gamma \in \{x, y, z\}$ and $\langle ij \rangle \in \alpha\beta(\gamma)$ mean that the bond plane of the nearest-neighbor bond $\langle ij \rangle$ is the $\alpha\beta$ -plane perpendicular to the γ -axis. We can expect $|K_z| \gg |K_x| = |K_y| \gtrsim J_x = J_y$ and $|K_z| \gtrsim J_z$ because the bond length in the xy -plane is shorter than the others. Then, we can treat the K_z and J_z terms as unperturbed parts, and K_x, K_y, J_x and J_y terms as perturbation. In the zeroth-order ground state, if $|K_z| > 2J_z$, the Ru ions connected by a blue circle in Fig. S6 will be dimerized ferromagnetically to $|\uparrow\rangle \otimes |\uparrow\rangle$ or $|\downarrow\rangle \otimes |\downarrow\rangle$. The perfect Kitaev model with $J_\gamma = 0$ will be mapped to the 2D toric code [11] if we see these dimers as pseudospins up and down, respectively, by using the fourth-order perturbation in K_x/K_z and K_y/K_z , and applying local unitary transformations. The ground state of the 2D toric code has a 2D Z_2 topological order and has fractionalized anyonic excitations. Even in the 3D case, a similar distorted heterogeneous structure is possible and the perfect 3D Kitaev model could be mapped to the 3D toric code in the same way as in the 2D case [12]. This model shows a 3D Z_2 topological order, which has string excitations with exotic statistics.

If we include the Heisenberg term, the situation is known to be different [13]. Even in the first order, there appears an antiferromagnetic Ising interaction $J_x S_i^z S_j^z$ between the pseudospins of two nearest-neighbor dimers i and j . Therefore, in order for the toric code stabilizer term to be dominant, we first have to impose the condition $K_x^2 K_y^2 / (16|K_z|^3) \gg J_x$ in this toric-code limit because the Ising term strongly favors a conventional Néel order for pseudospins, i.e. a stripy order for original $J_{\text{eff}} = 1/2$ spins. In addition, there appears a pseudospin flip interaction both from the second-order perturbation due to the J_z term and from the ignored Γ term, so we have to investigate whether or not these quantum fluctuations destroy the topological order similarly to the thermal fluctuation [14, 15] as an interesting future problem. In the heterogeneous case, the distortion due to the lack of the octahedral symmetry around Ru could make the effective model deviate from the JKT model more strongly than in the homogeneous case, but we can still expect an almost octahedral coordination if we use an amino-group in every direction as shown in Fig. S6.

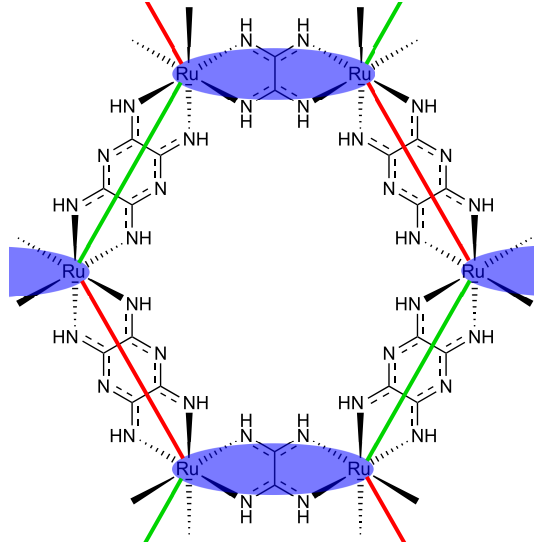


FIG. S6. Heterogeneous distorted honeycomb structure to realize a gapped spin liquid region. The bond interaction is shown with the same color as in Fig. 1(a) in the main text and the Ru ions connected by a blue circle will be dimerized.

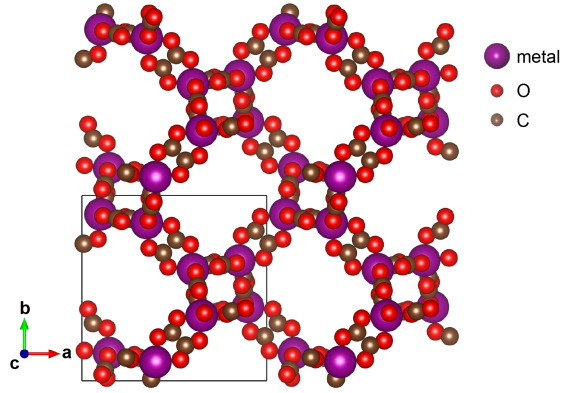


FIG. S7. (10,3)-*a* MOF with a $P4_132$ space group symmetry viewed from the [001] direction. While the ideal (10,3)-*a* should look like the square-octagon lattice when projected onto the (001) plane, the square spirals are tilted and, thus, regular octagons are distorted in two ways alternately in this figure. The unit cell is shown in the black solid line and it is clear to see this distortion breaks the translational symmetry with a vector $(\frac{1}{2}, \frac{1}{2}, \frac{1}{2})$. This figure is reconstructed from the crystal data included in Supporting Information of Ref. [16] (metal ions: purple, C: brown, O: red).

Section F: LATTICE DISTORTIONS IN THREE-DIMENSIONAL STRUCTURES

While a gapless nodal-line or Weyl spin liquid on (10,3)-*b* (the 3D hyperhoneycomb lattice) shown in Fig. S1 is stable against small lattice distortions, Majorana Fermi surfaces on (10,3)-*a* (the 3D hyperoctagon lattice) need protection by its $I4_132$ space group symmetry. For example, a (10,3)-*a* MOF with a space group $P4_132$, which is a subgroup of $I4_132$, has been realized [16], but the crystal system is lowered from a body-centered cubic system to a simple cubic system, which means that the unit cell of this real material is doubled from the ideal (10,3)-*a* lattice, as shown in Fig. S7. In this case, Fermi surfaces are unstable against an infinitesimal perturbation away from the $K_x = K_y$ line, i.e. the Majorana Fermi surfaces on (10,3)-*a* have to be protected by the translational symmetry with a vector $(\frac{1}{2}, \frac{1}{2}, \frac{1}{2})$ [17]. This difference between $I4_132$ and $P4_132$ comes from the fact that the reduced unit cell of the $I4_132$ structure is incommensurate with the bipartite coloring of (10,3)-*a*. We still need a further materials search for an ideal $I4_132$ structure to see quantum interaction effects on the Majorana Fermi surfaces [18].

-
- [1] K. Kitaura, T. Sawai, T. Asada, T. Nakano, and M. Uebayasi, *Chem. Phys. Lett.* **312**, 319 (1999).
 - [2] T. Ozaki, *Phys. Rev. B* **67**, 155108 (2003).
 - [3] J. P. Perdew, K. Burke, and M. Ernzerhof, *Phys. Rev. Lett.* **77**, 3865 (1996).
 - [4] F. H. Allen, *Acta Cryst.* **B58**, 380 (2002).
 - [5] B. Zhang, Y. Zhang, and D. Zhu, *Dalton Trans.* **41**, 8509 (2012).
 - [6] M. Itoi, A. Taira, M. Enomoto, N. Matsushita, N. Kojima, Y. Kobayashi, K. Asai, K. Koyama, T. Nakano, Y. Uwatoko, and J. Yamaura, *Solid State Commun.* **130**, 415 (2004).
 - [7] G. Jackeli and G. Khaliullin, *Phys. Rev. Lett.* **102**, 017205 (2009).
 - [8] S. M. Winter, Y. Li, H. O. Jeschke, and R. Valentí, *Phys. Rev. B* **93**, 214431 (2016).
 - [9] In Ref. [8], there is another term t_4 from xy to xz or yz , but we can ignore this contribution assuming the completely planar structure of molecule and the local mirror symmetry against this bond plane. This symmetry defines the distinction between π - and σ -orbitals and t_4 vanishes when they are independent.
 - [10] Ref. [8] defines these values for $4d^5$ metal ions in general. Therefore, we can expect that these values can be used not only for α - RuCl_3 , but also for MOFs.
 - [11] A. Kitaev, *Ann. Phys.* **303**, 2 (2003).
 - [12] S. Mandal and N. Surendran, *Phys. Rev. B* **90**, 104424 (2014).
 - [13] E. Sela, H.-C. Jiang, M. H. Gerlach, and S. Trebst, *Phys. Rev. B* **90**, 035113 (2014).
 - [14] S. Bravyi and B. Terhal, *New J. Phys.* **11**, 043029 (2009).
 - [15] B. Yoshida, *Ann. Phys.* **326**, 2566 (2011).
 - [16] E. Coronado, J. R. Galán-Mascarós, C. J. Gómez-García, and J. M. Martínez-Agudo, *Inorg. Chem.* **40**, 113 (2001).
 - [17] M. Hermanns and S. Trebst, *Phys. Rev. B* **89**, 235102 (2014).
 - [18] M. Hermanns, S. Trebst, and A. Rosch, *Phys. Rev. Lett.* **115**, 177205 (2015).